EasyChair Preprint

№ 10083

Estimation of Seismic Displacement Response Using a Kalman Filter with Data-Driven State-Space Model Identification

Yuki Kakiuchi, Yaohua Yang, Masaru Kitahara and Tomonori Nagayama

May 12, 2023

Estimation of seismic displacement response using a Kalman filter with data-driven state-space model identification

Yuki Kakiuchi[1], Yaohua Yang[1], Masaru Kitahara[1], and Tomonori Nagayama[1]

[1] Dept. of Civil Engineering, The University of Tokyo, Tokyo, Japan
nagayama@bridge.t.u-tokyo.ac.jp

Abstract. This paper proposes a system identification method combining a data-driven state-space model and the unscented Kalman filter (UKF) to estimate displacement time histories of systems with complex material nonlinearities under seismic excitations. In this method, the state-space equations are first constructed based on a series of polynomial functions using training data which are the dynamic responses generated from a finite element (FE) model with complex hysteresis behaviors. Specifically, the state-space equations are trained separately for the linear and nonlinear regions of the responses. Subsequently, the trained state-space equations are employed in the UKF to estimate the system displacements. In this stage, only the accelerations of the test data are regarded as observations. In the UKF, the time-variant process noise covariance matrix and the time-invariant measurement noise variance are inferred by the Robbins-Monro algorithm and the Markov chain Monte Carlo method, respectively. The proposed method is demonstrated on an FE bridge pier model using different input ground motions, and the results show that the proposed approach enables to accurately estimate the system displacements.

Keywords: Displacement estimation, State-space model identification, Data-driven approach, Unscented Kalman filter, Seismic response

1 Introduction

Rapid assessment of structure damages after an earthquake is of great importance from a safety and economic point of view. To evaluate the safety conditions of structures, displacement responses, especially the maximum displacement and the residual displacement, are preferable indicators. In practice, measuring structure displacement under seismic excitation still remains a challenging work. For example, a reliable stationary reference point is necessary for contact displacement sensor such as LVDTs [1], which is not practical for onsite application; Noncontact technologies, such as laser

scanning instruments, global position systems, and computer vision-based techniques possess the drawbacks of high-equipment cost, low sampling rate, low resolution and so on. Nowadays, comparing with displacement transducers, accelerometers are more widely employed for structural health monitoring. Displacements can also be estimated by integrating acceleration signals and applying appropriate high-pass filter [2], however, this approach cannot be applied to a system undergoing nonlinear deformations because the low-frequency components including the residual displacements are inevitably removed.

In addition, displacement estimation by combining measurement signals and system information has also been investigated, and the Kalman filter (KF) is one of the most attractive techniques. When a nonlinear system is represented in the KF, the system equations are usually defined using the assumed physical hysteresis model, and its parameters are inferred by e.g., the genetic algorithm [3] and the Markov chain Monte Carlo (MCMC) method [4]. However, when the model discrepancies are large, the estimation accuracies may deteriorate significantly. Alternatively, the system equations can also be obtained purely from input-output data. In the data-driven approach, the system equations are approximated by a series of basis functions without assuming an explicit hysteresis model. Ni et al. [5] approximated the state-space equation of a wire-cable isolator as a polynomial function in terms of displacement and hysteretic restoring force under cyclic loading. Lai and Nagarajaiah [6] developed a sparse system identification method, in which the state-space equations of systems with nonlinear hysteresis behavior under seismic excitation are approximated by sparse regression with the basis functions that include the input ground acceleration.

In this study, we augment the sparse system identification method by Lai and Nagarajaiah [6] by training the state-space equations separately for the linear and nonlinear system responses. Then, it is combined with the UKF to estimate the displacement of structures with complex material nonlinearities under seismic excitations. In the UKF, the process noise covariance matrix and the measurement noise variance are automatically estimated using Robbins-Monro (RM) algorithm and the MCMC method, respectively. The proposed approach is verified through a numerical example using a nonlinear finite element (FE) bridge pier model under various earthquake inputs. In the following, Section 2 outlines the detailed procedure of the proposed method; the numerical verifications are then presented in Section 3; finally, Section 4 gives the conclusions.

2 Nonlinear system identification under seismic excitation

2.1 Data-driven state-space model identification under seismic excitation

The equation of motion of a single degree-of-freedom (DOF) system is written as:

$$\begin{cases} m\ddot{x} + f_h = -m\ddot{x}_g \\ \dot{f}_h = g(x, \dot{x}, f_h) \end{cases} \tag{1}$$

where m denotes the mass; x is the relative displacement; $\ddot{x}_g$ is the input ground acceleration; f_h is the nonlinear restoring force which also includes structural damping. This equation of motion can be represented as a state-space model:

$$\dot{\boldsymbol{x}} = f(\boldsymbol{x}, \ddot{x}_g) = \begin{bmatrix} \dot{x} \\ -a_h - \ddot{x}_g \\ \frac{1}{m} g(x, \dot{x}, m a_h) \end{bmatrix} \tag{2}$$

where

$$\boldsymbol{x} = \begin{bmatrix} x \\ \dot{x} \\ a_h \end{bmatrix} \tag{3}$$

where a_h is the absolute acceleration, which is calculated as the negative sum of the relative acceleration $\ddot{x}$ and the input ground acceleration $\ddot{x}_g$. According to Lai and Nagarajaiah [6], the nonlinear system function f can be approximated by the sum of basis function as follows:

$$\dot{\boldsymbol{x}} = \boldsymbol{\Xi}\left[\boldsymbol{\Theta}(\boldsymbol{x}, \ddot{x}_g)\right]' \tag{4}$$

where $\boldsymbol{\Theta}$ denotes the assembly of the basis functions; $\boldsymbol{\Xi}$ is the corresponding coefficient matrix. Specifically, the assembly $\boldsymbol{\Theta}$ can be written as:

$$\boldsymbol{\Theta}(\boldsymbol{x}, \ddot{x}_g) = \left[1 \; \boldsymbol{X} \; \boldsymbol{X}^2 \; \cdots \; \ddot{x}_g\right] \tag{5}$$

where $\boldsymbol{X} = [x \; \dot{x} \; a_h \; |\dot{x}| \; |a_h|]$; $\boldsymbol{X}^i$ $(i = 2, 3, \cdots)$ is the higher-order polynomial terms. For example, $\boldsymbol{X}^2$ is the second-order polynomial terms expressed as:

$$\boldsymbol{X}^2 = [x^2 \; \cdots \; |a_h|^2 \; x\dot{x} \; \cdots \; x|a_h| \; \dot{x}a_h \; \cdots \; |\dot{x}||a_h|] \tag{6}$$

In this study, $\dot{\boldsymbol{x}}$ and $\boldsymbol{\Theta}(\boldsymbol{x}, \ddot{x}_g)$ are both computed using a numerical model of the target system. Based on these artificially generated seismic response data, the coefficient matrix $\boldsymbol{\Xi}$ can be estimated by sparse regression using the LASSO algorithm [7]. The highest order of the polynomial terms and the regularization factor in the LASSO algorithm are determined based on Akaike information criterion (AIC). The reader can refer to Lai and Nagarajaiah [6] for the detailed procedure of sparse regression.

Under strong seismic excitation, the third row in $\boldsymbol{\Xi}$ can differ for the linear and nonlinear regions of the system responses. Hence, the seismic response data $\dot{\boldsymbol{x}}$ and $\boldsymbol{\Theta}(\boldsymbol{x}, \ddot{x}_g)$ are divided into three sections: region A before the nonlinear responses are observed; region B where the input ground motion increases and the nonlinear responses are observed; region C after the nonlinear responses are finished. Then, the state equation of each region is estimated, respectively, as follows:

$$\dot{\boldsymbol{x}}_k = \boldsymbol{\Xi}_{lasso}\left[\boldsymbol{\Theta}(\boldsymbol{x}_k, \ddot{x}_{gk})\right]' \tag{7}$$

where

$$\boldsymbol{\Xi}_{lasso} = \begin{cases} \boldsymbol{\Xi}_{A,lasso} & (1 \le k \le T_a) \\ \boldsymbol{\Xi}_{B,lasso} & (T_a + 1 \le k \le T_b) \\ \boldsymbol{\Xi}_{C,lasso} & (T_b + 1 \le k \le T) \end{cases} \tag{8}$$

where T_a and T_b denote the time where the Sections A and B are finished, respectively; T is the total length of the discrete input ground motion. In this paper, T_a and T_b are determined manually from the datasets. It is noted that, they can also be automatically estimated by identifying the time-variant system stiffness [8, 9] or the natural frequency history of the system [10].

2.2 Displacement estimation by UKF

Based on the state-space model derived in the previous section, the UKF [11] is utilized to estimate the system displacement using available observations.

The state equation and the observation equation are expressed as follows:

$$\dot{\boldsymbol{x}}_k = \boldsymbol{\Xi}_{lasso}\left[\boldsymbol{\Theta}\left(\boldsymbol{x}_k, \ddot{x}_{gk}\right)\right]' + \boldsymbol{v}_k \tag{9}$$

$$y_k = \boldsymbol{C}\dot{\boldsymbol{x}}_k + w_k \tag{10}$$

where $\boldsymbol{v}_k$ and w_k represent the process noise and observation noise, respectively; y_k denotes the observations; $\boldsymbol{C}$ indicates the observation matrix. In this study, the absolute acceleration of the system is employed as the observations; thus, $\boldsymbol{C}$ is a simple selection matrix:

$$\boldsymbol{C} = [0 \quad 0 \quad 1] \tag{11}$$

In the UKF, the state estimate $\widehat{\boldsymbol{x}}_{k+1}$ is obtained as:

$$\widehat{\boldsymbol{x}}_{k+1} = \widehat{\boldsymbol{x}}_{k+1}^{-} + \boldsymbol{G}_{k+1}(y_{k+1} - \hat{y}_{k+1}^{-}) \tag{12}$$

where $\widehat{\boldsymbol{x}}_{k+1}^{-}$ denotes the prior state estimate; $\boldsymbol{G}_{k+1}$ is the Kalman gain; $\hat{y}_{k+1}^{-} = \boldsymbol{C}\widehat{\boldsymbol{x}}_{k+1}^{-}$ is the prior estimate of the observation quantities. The prior state estimate $\widehat{\boldsymbol{x}}_{k+1}^{-}$ is obtained from a total of $2n + 1$ sigma points $\boldsymbol{\mathcal{X}}_{i,k+1}^{-}$ $(i = 1, \cdots, 2n + 1)$ that are computed based on the time integration of the state-space equation in Eq. (7). In this study, the Runge-Kutta method is used to perform the time integration. In addition, the Kalman gain $\boldsymbol{G}_{k+1}$ is computed as follows:

$$\boldsymbol{G}_{k+1} = \boldsymbol{P}_{k+1}^{-}\boldsymbol{C}'\{\boldsymbol{C}\boldsymbol{P}_{k+1}^{-}\boldsymbol{C}' + R\}^{-1} \tag{13}$$

where $\boldsymbol{P}_{k+1}^{-}$ indicates the prior estimate of the error covariance matrix that is obtained based on the prior state estimate $\widehat{\boldsymbol{x}}_{k+1}^{-}$, the sigma points $\boldsymbol{\mathcal{X}}_{i,k+1}^{-}$, and the process noise covariance matrix $\boldsymbol{Q}_k$; $\boldsymbol{R}$ is the observation noise variances.

After the UKF procedure, the Rauch-Tung-Striebel (RTS) smoothing [12] is further performed to obtain the smoothed state estimate:

$$\widehat{\boldsymbol{x}}_k^{smth} = \widehat{\boldsymbol{x}}_k + \boldsymbol{G}_k^{smth}\left(\widehat{\boldsymbol{x}}_{k+1}^{smth} - \widehat{\boldsymbol{x}}_{k+1}^{-}\right) \tag{14}$$

where $\boldsymbol{G}_k^{smth}$ is the Kalman gain in the smoothing. The reader can refer to Särkkä [12] for the detailed procedures of the UKF and RTS smoothing. It should be noted that, in the following sections, the UKF refers to both the filtering and smoothing procedures, and $\hat{\boldsymbol{x}}_k^{smth}$ (i.e., the first component in $\hat{\boldsymbol{x}}_k^{smth}$) is used as the displacement estimate.

2.3 Process noise and observation noise estimation

To improve the performance of the UKF, the appropriate settings for process noise and observation noise are important. In this study, they are assumed to follow zero mean independent Gaussian distributions, and the process noise covariance matrix $\boldsymbol{Q}_k$ and the observation noise variance R are estimated by the RM algorithm and the MCMC algorithm, respectively. Note that, the process noise covariance matrix is time-variant while the observation noise variance is a constant value.

In the RM algorithm, the process noise covariance matrix is obtained as follows:

$$\boldsymbol{Q}_{k+1} = (1-\alpha_Q)\boldsymbol{Q}_k + diag\{\alpha_Q \boldsymbol{G}_{k+1}(y_{k+1} - \hat{y}_{k+1}^-)(y_{k+1} - \hat{y}_{k+1}^-)'\boldsymbol{G}_{k+1}'\} \quad (15)$$

where $diag$ denotes the diagonal elements estimator; α_Q is a constant value controlling the degree of difference between $\boldsymbol{Q}_k$ and $\boldsymbol{Q}_{k+1}$. In this study, it is selected from 1/5, 1/20, 1/50, 1/100, 1/200, and 1/400 to achieve the optimal state estimation.

In the MCMC algorithm, on the other hand, the UKF process is performed iteratively to obtain a chain of R with the length of m, i.e., $\{\boldsymbol{R}\}_{i=1}^m$. The candidate sample R_{i+1}^- is generated from a Gaussian proposal distribution with the standard deviation σ_R:

$$R_{i+1}^- \sim \mathcal{N}(R_i, \sigma_R) \quad (16)$$

The likelihood of the candidate sample can be then computed as:

$$\log \Phi_{i+1}^- = \sum_{k=1}^T \log \varphi_{i+1,k} \quad (17)$$

with

$$\log \varphi_{i+1,k} = -\frac{1}{2}\log\{2\pi(\boldsymbol{C}\boldsymbol{P}_k^-\boldsymbol{C}' + R_{i+1}^-)\} - \left(\frac{y_k - \hat{y}_k^-}{\boldsymbol{C}\boldsymbol{P}_k^-\boldsymbol{C}' + R_{i+1}^-}\right)^2 \quad (18)$$

The candidate sample is accepted with probability α defined as:

$$\alpha = \min\left[1, \frac{\Phi_{i+1}^-}{\Phi_i}\right] \quad (19)$$

where Φ_i denotes the likelihood of the ith sample R_i. In practice, a random value r is generated from a standard uniform distribution (i.e., $r \sim U[0,1]$). If $\alpha \geq r$, the candidate sample R_{i+1}^- is accepted (i.e., $R_{i+1} = R_{i+1}^-$). Otherwise, R_{i+1}^- is rejected (i.e., $R_{i+1} = R_i$). Finally, the estimator, $\hat{R}$, of the observation noise variance which maximizes the likelihood $\{\Phi\}_{i=1}^m$ is obtained.

3 Numerical application

The proposed framework is demonstrated on a numerical example using the bridge pier FE model shown in Fig. 1. This model is originally studied in Ebrahimian et al. [13] based on fiber elements, but shell elements with elastic and inelastic materials are used here. The material properties are summarized in Tables 1 and 2, in which the nonlinear material properties are determined based on Hartloper et al. [14].

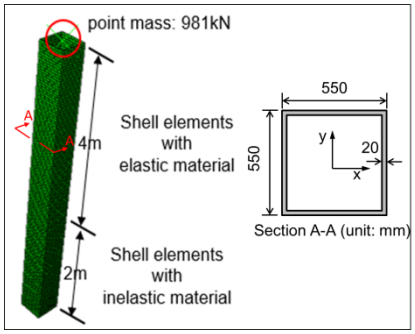

Fig. 1. Overview of the bridge pier FE model

Table 1. Description of the linear material properties.

Young's Modulus	Poisson's ratio	Mass density	Rayleigh damping coefficient α	Rayleigh damping coefficient β
2.0×10^{11} N/m^2	0.3	7800 kg/m^3	0.7392	0.0006

Table 2. Description of the nonlinear material properties.

Yield stress at zero plastic strain	Kinematic hardening magnitude C_1	Kinematic hardening magnitude C_2	Kinematic hardening rate γ_1	Kinematic hardening rate γ_2	Isotropic hardening magnitude Q_∞	Isotropic hardening rate
3.39×10^8 Pa	2.62×10^{10}	2.45×10^9	199.04	11.66	1.34×10^8 Pa	14.71

In this study, five ground motion records, namely Takatori, Northridge, JMA Kobe, San Fernando, and Imperial Valley, are employed, which are available from the website of Center for Engineering Strong Motion Data (https://www.strongmotioncenter.org/). These records are first scaled so that their peak ground accelerations equal 800 gal; then they are applied to the FE model in the *x*-direction to conduct the forward dynamic simulations. The simulated responses at the point-mass node, i.e., the relative displacements, the relative velocities, and the absolute accelerations in the *x*-direction, are employed as training and test data. Specifically, the datasets generated by the first three records

consisting of $\dot{\boldsymbol{x}}$ and $\boldsymbol{\Theta}(\boldsymbol{x}, \ddot{x}_g)$ are used to train the state-space equation in Eq. (7), while the absolute accelerations from the latter two records are regarded as the observations in the UKF to estimate the displacements at the point-mass node. In particular, to remove the high-frequency components in $\dot{a}_h$ due to numerical derivative, a low-pass filter with the upper limit of 25 Hz is applied to the datasets.

The results of sparse regression based on the LASSO algorithm are illustrated for Section B in Fig. 2a and for Section C in Fig. 2b, respectively. Similar results as Section C are obtained for Section A and hence they are not presented in Fig. 2. The upper two figures show the AIC values for the third line in the state-space equation with different regularization factor λ. In this study, the maximum order of the polynomial terms in Eq. (5) is changed from one to six so as to determine the optimal assembly $\boldsymbol{\Theta}$.

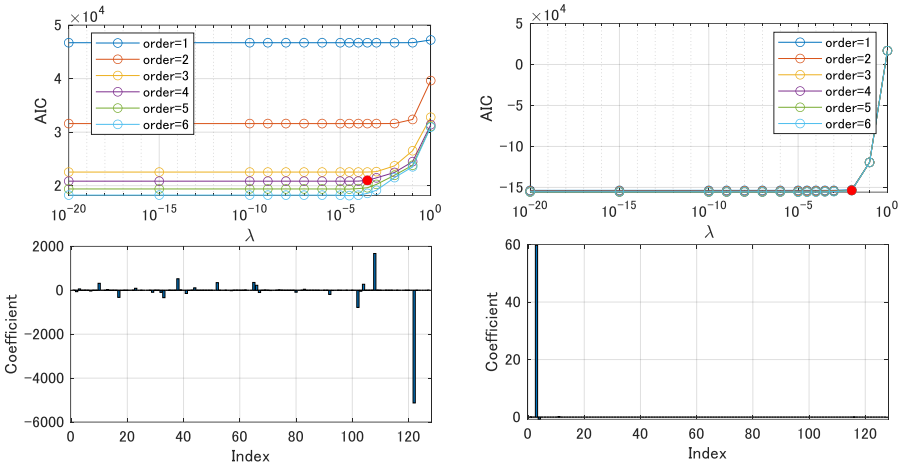

Fig. 2. Sparse regression results: (a) Section B (nonlinear region), (b) Section C (linear region).

For Section B (i.e., nonlinear region), it is observed that the AIC values decrease when higher-order polynomial terms are considered. However, differences in the AIC values are marginal for orders 4, 5, and 6. Hence, the assembly $\boldsymbol{\Theta}$ up to the four-order polynomial terms is employed to avoid overfitting. The optimal regularization factor is then selected as the turning point of the AIC curve that is denoted by the red point in Fig. 2. The estimated coefficients are detailed in the lower figure, where the horizontal axis corresponds to the index of the basis terms. It can be seen that the coefficients of several terms in $\boldsymbol{\Theta}$ including higher-order terms are non-zero, indicating that complex hysteresis behavior is observed.

For Section C (i.e., linear region), on the other hand, it is observed that differences in the AIC values are marginal for all orders. Thus, only the linear basis terms are used to approximate the state-space equation. In the derived equation, only three components $\dot{x}$, a_h, and $|\dot{x}|$ have non-zero coefficients.

The trained state-space equation is then used to perform the UKF procedure. Fig. 3 shows the estimated displacement responses at the point-mass node and corresponding hysteresis loops. The results for the Takatori ground motion record are shown in Fig. 3a to demonstrate the approximation accuracy of the proposed approach for training data. On the other hand, the results for San Fernando ground motion record are depicted in Fig. 3b to demonstrate the prediction accuracy of the proposed approach for test data. Furthermore, the results obtained by performing the time integration without applying the UKF are also shown in Fig. 3 for comparison purpose.

From the results without applying the UKF in Fig. 3a, it can be observed that the overall approximation accuracy of the trained state-space equation is sufficient including the residual displacements. However, the approximation accuracy is still not sufficient for the maximum displacement. This can be also found in Table 3 where the estimation errors are summarized in terms of the maximum relative error and the root mean square error (RMSE). For all the training data, the RMSE is less than 10 % but the maximum relative error is larger than 15 % for Takatori and Northridge ground motion records. Besides, it can be observed from Fig. 3b that the prediction accuracy of the trained state-space equation is also not sufficient for the residual displacements of the test data.

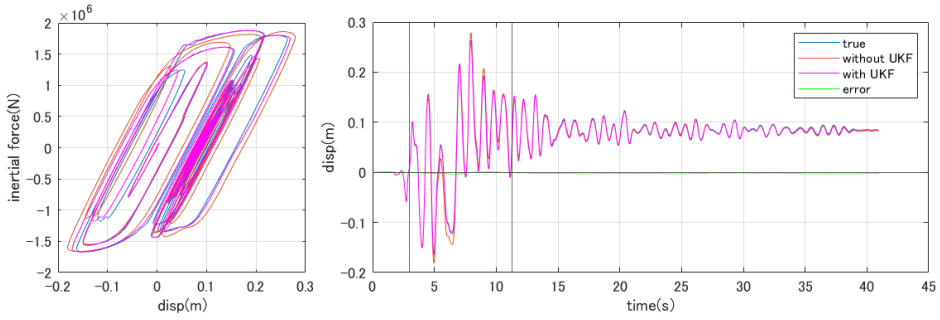

(a)

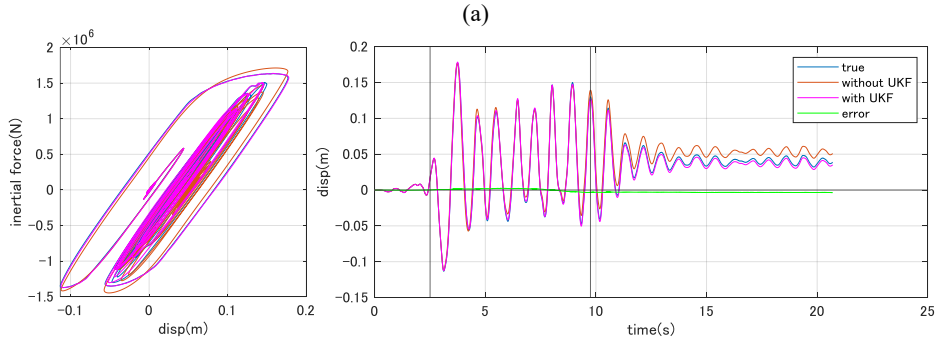

(b)

Fig. 3. The estimated displacement and hysteresis loop: (a) Takatori, (b) San Fernando.

Table 3. Estimation error for different ground motion records.

	Earthquake record	Maximum relative error (%)		RMSE (%)	
		Without UKF	With UKF	Without UKF	With UKF
Training data	Takatori	15.1	1.4	2.8	0.4
	Northridge	22.6	3.7	9.5	1.5
	JMA Kobe	5.1	1.3	1.6	0.4
Test data	San Fernando	10.1	2.0	3.6	1.2
	Imperial Valley	6.6	3.0	1.0	1.1

Compared to the results without applying the UKF, the estimated displacements by the UKF show favorable agreement with the true displacement responses both for the training and test data. It can be seen in Table 3 that the maximum relative errors and the RMSEs are less than 4 % for all the cases, indicating that the proposed approach enables to appropriately infer the seismic displacement of the system including the maximum displacement and residual displacement.

4 Conclusion

In this paper, a displacement estimation method for systems with complex material nonlinearities under seismic excitations is developed combining the data-driven state-space model identification and the UKF. In this method, the state-space equations for the nonlinear system are first constructed using training data that are generated from the numerical model of the target system. The UKF is then applied with the trained state-space equation to estimate the displacements when only acceleration observations are available. Specifically, the state-space equations are trained for the linear and nonlinear regions separately to enhance the model stability. Furthermore, in the UKF, the process noise covariance matrix and the observation noise variance are estimated using the RM algorithm and the MCMC algorithm, respectively, to further improve the displacement estimation accuracies. A nonlinear FE bridge pier model is used to demonstrate the proposed approach. Compared to the forward time integration of the derived state-space model, the proposed approach can appropriately estimate the system displacements by the UKF updating with the acceleration observations.

References

1. Szewczyk, P., Kudyba, P.: Effectiveness of selected strain and displacement measurement techniques in Civil Engineering. Buildings 12(2), 172 (2022).
2. Gindy, M., Nassif, H. H., Velde, J.: Bridge displacement estimates from measured acceleration records. Transportation research record 2028(1), 136-145 (2007).

3. Ishihara, K., Yang, Y., Nagayama, T., Nakamura, T., Su, D.: Displacement response estimation based on measurement of acceleration response and nonlinear hysteresis model. JSCE Journal of Structural Engineering 68A, 275-288 (2022). (In Japanese.)
4. Kuno, H.: Bayesian estimation of displacement and structural parameters using state space model and Pseudo-Marginal MCMC for structural damage assessment, Master thesis, Dept. of Civil Engineering, Univ. of Tokyo (2020). (In Japanese.)
5. Ni, Y.Q., Ko, J.M., Wang, C.W.: Nonparametric identification of nonlinear hysteretic systems. Journal of Engineering Mechanics 125(2), 206-215 (1999).
6. Lai, Z., Nagarajaiah, S.: Sparse structural system identification method for nonlinear dynamic systems with hysteresis/inelastic behavior. Mechanical Systems and Signal Processing 117, 813-842 (2019).
7. James, G., Witten, D., Hastie, T., Tibshirani, R.: An introduction to statistical learning. Vol 6. Springer, New York (2013).
8. Yang, Y., Nagayama, T., Xue, K., Su, D.: Displacement estimation of a nonlinear SDOF system under seismic excitation using an adaptive Kalman filter. ASCE-ASME Journal of Risk and Uncertainty in Engineering Systems, Part A: Civil Engineering 8(1), 04021084 (2022).
9. Yang, Y., Nagayama, T., Xue, K.: Structure system estimation under seismic excitation with an adaptive extended Kalan filter. Journal of Sound and Vibration 489, 115690 (2020).
10. Takeda, T.: Reproduction of long-span bridge seismic responses involving tower-girder pounding and damage process estimation for large earthquakes, Doctor thesis, Dept. of Civil Engineering, Univ. of Tokyo (2017). (In Japanese.)
11. Erazo, K., Nagarajaiah, S: An offline approach for output-only Bayesian identification of stochastic nonlinear systems using unscented Kalman filtering. Journal of Sound and Vibration 397, 222-240 (2017).
12. Särkkä, S.: Bayesian filtering and smoothing. Vol 3. Cambridge University Press (2013).
13. Ebrahimian, H., Astroza, R., Conte J.P.: Extended Kalman filter for material parameter estimation in nonlinear structural finite element models using direct differentiation method. Earthquake Engineering & Structural Dynamics 44(10), 1495-1522 (2015).
14. Hartloper, A.R., Sousa, A.C., Lignos, D.G.: Constitutive modeling of structural steels: nonlinear isotropic/kinematic hardening material model and its calibration. Journal of Structural Engineering 147(4), 04021031 (2021).